

Most hard X-ray selected quasars in *Chandra* Deep Fields are obscured

J. X. Wang¹, P. Jiang¹, Z. Y. Zheng¹, P. Tozzi^{2,3}, C. Norman^{4,9}, R. Giacconi⁴, R. Gilli⁵, G. Hasinger⁶, L. Kewley⁷, V. Mainieri⁶, M. Nonino³, P. Rosati⁸, A. Streblyanska⁶, G. Szokoly⁶, A. Zirm⁴, W. Zheng⁴

ABSTRACT

Measuring the population of obscured quasars is one of the key issues to understand the evolution of active galactic nuclei (AGNs). With a redshift completeness of 99%, the X-ray sources detected in *Chandra* Deep Field South (CDF-S) provide the best sample for this issue. In this letter we study the population of obscured quasars in CDF-S by choosing the 4 – 7 keV selected sample, which is less biased by the intrinsic X-ray absorption. The 4 – 7 keV band selected samples also filter out most of the X-ray faint sources with too few counts, for which the measurements of N_H and L_X have very large uncertainties. Simply adopting the best-fit $L_{2-10keV}$ and N_H , we find $71 \pm 19\%$ (20 out of 28) of the quasars (with intrinsic $L_{2-10keV} > 10^{44}$ erg s⁻¹) are obscured with $N_H > 10^{22}$ cm⁻². Taking account of the uncertainties in the measurements of both N_H and L_X , conservative lower and upper limits of the fraction are 54% (13 out 24) and 84% (31 out 37). In *Chandra* Deep Field North, the number is 29%, however, this is mainly due to the redshift incompleteness. We estimate a fraction of $\sim 50\% - 63\%$ after correcting the redshift incompleteness with a straightforward

¹Center for Astrophysics, University of Science and Technology of China, Hefei, Anhui 230026, P. R. China; jxw@ustc.edu.cn.

²INAF Osservatorio Astronomico, Via G. Tiepolo 11, 34131 Trieste, Italy

³INFN - National Institute for Nuclear Physics, Trieste, Italy

⁴Dept. of Physics and Astronomy, The Johns Hopkins University, Baltimore, MD 21218

⁵Istituto Nazionale di Astrofisica (INAF) - Osservatorio Astrofisico di Arcetri, Largo E. Fermi 5, 50125 Firenze, Italy

⁶Max-Planck-Institut für extraterrestrische Physik, Postfach 1312, D-85741 Garching, Germany

⁷Hubble Fellow, Institute for Astronomy, University of Hawaii, 2680 Woodlawn Drive, Manoa, HI 96822

⁸European Southern Observatory, Karl-Schwarzschild-Strasse 2, Garching, D-85748, Germany

⁹Space Telescope Science Institute, 3700 San Martin Drive, Baltimore, MD 21218

approach. Our results robustly confirm the existence of a large population of obscured quasars.

Subject headings: surveys — galaxies: active — quasars: general — X-rays: galaxies

1. Introduction

Supermassive black holes (SMBH) have been found in the center of most (if not all) nearby galaxies (e.g. Kormendy & Richstone 1995; Kormendy & Gebhardt 2001), the growth of which is believed mainly due to the accretion of quasars (e.g., luminous active galactic nuclei) in the distant universe (Yu & Tremaine 2002). The unified model for active galactic nuclei (AGNs; Antonucci 1993) has predicted a large population of heavily obscured powerful quasars called type-2 quasars. They have been predicted to be the same as type-1 quasars but with strong obscuration in both optical and soft X-ray band. Most of such type-2 quasars, which might dominate the black hole growth (e.g., Martínez-Sansigre et al. 2005), have been missed by optical surveys for quasars.

The hard X-ray emission is less biased by the obscuration, making hard X-ray surveys a good approach to search for type-2 quasars. Recent deep and wide-area X-ray surveys performed by *Chandra* and XMM have revealed a number of such sources (Norman et al. 2002; Stern et al. 2002; Mainieri et al. 2002; Fiore et al. 2003; Caccianiga et al. 2004). Using various *Chandra* and *ASCA* surveys, Steffen et al. (2003) claimed that broad-line sources dominate above $L_{2-8keV} = 3 \times 10^{43}$ ergs s^{-1} , and type II AGNs become important only at Seyfert-like X-ray luminosities. Similarly, Ueda et al. (2003) computed the X-ray luminosity function for 2 – 10 keV selected AGN samples, and found that the fraction of X-ray absorbed AGNs (with $N_H > 10^{22}$ cm^{-2}) drops from ~ 0.6 at intrinsic L_X around 10^{42} ergs s^{-1} to around 0.3 at L_X above 10^{44} ergs s^{-1} . Several other studies based on hard X-ray surveys also support the scheme that the fraction of type II AGNs (or X-ray absorbed AGNs) decreases with intrinsic luminosity (Barger et al. 2005; La Franca et al. 2005). However, contrary results are also reported. By performing Monte-Carlo simulations to match the X-ray colors in the 13^H *XMM-Newton* deep field, Dwelly et al. (2005) claimed that the fraction of obscured AGN depends on neither the luminosity nor the redshift. Perola et al. (2004) found that the fraction of obscured AGNs in HELLAS2XMM does not change with X-ray luminosity, although the fraction (40%) appears smaller than expected. Also see Eckart et al. (2006) and Dwelly & Page (2006) for most recent works. Note that the observed fraction of obscured sources is a function of the X-ray flux due to the bias of the absorption and/or its evolution with redshift (see e.g. Comastri et al. 2001; Piconcelli et al. 2002, 2003; Ueda

et al. 2003; La Franca et al. 2005), therefore one should be cautious to compare results from surveys with different depths.

The 2 Ms *Chandra* exposure on *Chandra* Deep Field North (CDF-N, Brandt et al. 2001; Alexander et al. 2003) and 1 Ms exposure on *Chandra* Deep Field South (CDF-S, Giacconi et al. 2002) are the deepest X-ray images ever taken. Tozzi et al. (2006, hereafter T06) presented the detailed X-ray spectral studies and obtained absorption corrected luminosities (which is essential for the identification of quasars) for the X-ray sources in CDF-S. In this letter, we present samples of 4 – 7 keV band selected AGNs in *Chandra* Deep Fields, and employed such samples to study the population of obscured quasars. We point out that comparing with the normally used hard band (2 – 7/8/10 keV), 4 – 7 keV band samples are less biased against X-ray photo-electronic absorption, therefore are better suited to study the fraction of obscured sources. Throughout this paper, H_0 is taken to be $70 \text{ ks s}^{-1} \text{ Mpc}^{-1}$, $\Omega_m=0.3$ and $\Omega_\lambda=0.7$ (Spergel et al. 2003).

2. The X-ray Data Reduction

The 1 Ms *Chandra* exposure on the CDF-S was composed of eleven individual ACIS observations obtained from October 1999 to December 2000. The detailed data reduction and analysis are described in Giacconi et al. (2001; 2002), Tozzi et al. (2001) and Rosati et al. (2002). An X-ray catalog of 347 X-ray sources was presented in Giacconi et al. (2002). The 2 Ms *Chandra* exposure on the CDF-N was composed of twenty individual ACIS observations obtained from November 1999 to February 2002 (Alexander et al. 2003). An X-ray catalog of 503 X-ray sources was presented in Alexander et al. (2003).

In this letter we use updated X-ray data reductions with CIAO3.2.2 and CALDB3.1.0 on both CDF-S and CDF-N, therefore including the most updated corrections. For each individual observation, the ACIS hot pixels and cosmic ray afterglows were re-identified using the new CIAO script “*acis_run_hotpix*”. The level 1 data were then reprocessed to clean the ACIS particle background for both FAINT and VFAINT mode observations, and filtered to include only the standard event grades 0,2,3,4,6. The recently released time-dependent gain correction and ACIS charge transfer inefficiency (CTI) correction were also applied. Due to the large off-axis angle during the observations, the ACIS-S chips have poorer spatial resolution and effective area than the ACIS-I chips. In this paper, data from any ACIS-S CCD are ignored. All bad pixels and columns were also removed. High background time intervals were finally removed from level 2 files. The offsets between the astrometry of individual observations were obtained by registering the X-ray sources showing up in both exposures. 4 – 7 keV band X-ray images were extracted from the combined event files for

the two fields.

We run WAVDETECT (Freeman et al. 2002) on the extracted 4 – 7 keV band X-ray images using a probability threshold of 1×10^{-7} (corresponding to 0.5 false sources expected per image), and wavelet scales of 1, $\sqrt{2}$, 2, $2\sqrt{2}$, 4, $4\sqrt{2}$, 8, $8\sqrt{2}$, 16 pixels (1 pixel = $0.492''$). A total of 107 X-ray sources were detected in 4 – 7 keV band in CDF-S and 176 in CDF-N. We state that no new sources were detected in addition to the published catalogs. Rosati et al. (2002) stated that 110 X-ray sources in CDF-S show $S/N > 2.1$ in 5 – 7 keV band, however, these sources are pre-selected by running SExtractor on the 0.5 – 7 keV band image and filtered with X-ray photometry measurements, thus are not selected independently in the 5 – 7 keV band and are biased by softer band brighter sources which have higher chance to be pre-selected by SExtractor. By comparing with the catalogs in Szokoly et al. (2004) and Zheng et al. (2004), we got the spectroscopic/photometric redshifts for all the 107 sources in CDF-S. 54 out of them have secure spectroscopic redshifts, and for sources with photometric redshifts, a medium uncertainty (at 95% confidence level) of 0.17 in the redshift is expected. Considering that we are studying quasars which are located at much higher redshifts, the uncertainties in the redshift won't significantly affect our main results in this paper. We also make a quick estimation on the reliability of the optical counterparts. Zheng et al. (2004) provides the offsets of counterparts from X-ray positions. Taking the offsets as radius of circles, the total area within the circles are 918 square arc seconds for our 107 X-ray sources, and there are at most 7 random sources (down to $R = 26$, assuming a density of 100,000 per square degree) in such a region. Considering that most of X-ray sources have optical counterparts much brighter than $R=26$ which could outshine fainter spurious sources, and a large fraction of them have been confirmed to be AGN by optical spectra, the true number of spurious optical counterparts within our 107 sources is much smaller than 7, thus will not either affect our main results presented in this paper.

Following T06 we perform X-ray spectral fitting to obtain their X-ray absorption column density, and absorption corrected rest frame 2 – 10 keV luminosities. The source spectrum was extracted from a circle of radius $R_s = 2.4 \times FWHM$ and the background extracted from an annulus with outer radius R_s+12'' and inner radius R_s+2'' , after masking out other sources. XSPEC11.3.1 and Cash statistics were adopted to perform the spectral fits in 0.6 – 7.0 keV band. We found that our own fitting results are consistent (within the fitting uncertainty, see Fig. 1) with T06 which used an earlier version of *Chandra* calibration CALDB2.26 and CIAO3.0.1. This indicates that the uncertainty in the data calibration does not significantly affect our results presented in this paper. For the 176 X-ray sources in CDF-N, we got 127 spectroscopic/photometric redshifts from Barger et al. (2003), yielding a redshift completeness of 72%.

3. Why 4 – 7 keV?

It's well known that harder band X-ray emission is less affected by photo-electronic absorption, thus the harder X-ray band is less biased against absorption, and is best suited to select obscured sources (Fiore et al. 1999; Comastri et al. 2001; Nandra et al. 2003)¹. In this paper, we choose to adopt the 4 – 7 keV selected sample to study the population of obscured quasars in CDFs. Since 4 – 7 keV band is less biased against the absorption than the traditional 2 – 7/8 keV band, the observed fraction of obscured quasars in this band is less biased and is expected to be closer to the true value.

Another significant advantage of using 4 – 7 keV band sample is to filter out faint sources with too few X-ray counts, for which the X-ray spectral fitting yield too large uncertainties and could produce artificial high absorption and luminosity (especially at high z , see simulations in T06). In Fig. 2 we plot N_H versus 2 – 7 keV band counts for the 2 – 7 keV selected sources in CDF-S (open squares). The 107 4 – 7 keV band detected sources are overplotted as solid squares. Comparing with a 2 – 7 keV counts limited bright sample with the same number of sources, the 4 – 7 keV band sample picked up more sources with $N_H \gtrsim 10^{23} \text{ cm}^{-2}$, thus is clearly more complete to obscured sources. The 4 – 7 keV band sample also filters out most of faint X-ray sources with very few counts, making it more suitable for X-ray spectral analysis.

During the spectral fit, we do not fix the photon index Γ at 1.8, but allow it vary from 1.4 to 2.4 for faint sources (since too low or too high values might not be physical). This is because a) while an average $\Gamma = 1.8$ is valid for an AGN sample, the fitting results for individual sources could be strongly biased due to the scattering of Γ ; b) the uncertainties in the measurements could be significantly underestimated by fixing Γ . The fitting results are shown in table 1. We also point out that the measurements of the intrinsic L_X also have large uncertainties, especially for faint and obscured sources. In Fig. 3 we plot the 90% confidence region ($\Delta C = 2.706$) of N_H and L_X for two faint sources (which would be classified as obscured quasars in T06). Instead of fixing the photon index at 1.8, the confidence region was calculated by setting the photon index free (varying from 1.4 to 2.4). In the figure we can clearly see the large uncertainties in the measurement of L_X and N_H which both should also be taken into account while classifying obscured quasars. We can also see the potential bias caused to the measurement of N_H and L_X by fixing Γ at 1.8. In Fig. 4 we plot the best fit N_H obtained with Γ free versus that with Γ fixed at 1.8. We can clearly see that fixing Γ at 1.8 introduces obvious scattering for individual sources in the measurement of N_H ,

¹ Note this is not true for Compton-thick sources, since for Compton-thick absorption, even γ -ray emission could be strongly biased by Compton scattering, see Wang & Jiang 2006).

although there is no systematic difference between two values. Fixing Γ also significantly underestimate the uncertainty of N_H , which would also lead to obvious uncertainty in the measurement of L_X (see Fig. 3).

4. The fraction of obscured quasars

The output N_H versus L_X for 107 sources selected in 4 – 7 keV band in CDF-S is presented in Fig. 5. Our selection criteria for obscured quasars ($L_{2-10keV} > 10^{44}$ erg s $^{-1}$ and $N_H > 10^{22}$ cm $^{-2}$) are also plotted. Among the 107 sources, we identify 13 secure obscured quasars (XID 18,25,27,35,45,57,62,68,72,76,153,159,202) with both $L_{2-10keV} > 10^{44}$ erg s $^{-1}$ and $N_H > 10^{22}$ cm $^{-2}$ at $> 90\%$ confidence level and 6 secure unobscured quasars (XID 11,22,42,60,67,206). There are 5 more quasars (XID 6,7,24,31,61) with $L_{2-10keV} > 10^{44}$ erg s $^{-1}$ at $> 90\%$ confidence level but 90% N_H uncertainty range across 10^{22} cm $^{-2}$. A conservative lower limit in the fraction of X-ray obscured quasars (with $N_H > 10^{22}$ cm $^{-2}$) is thus 54%. Considering there are 13 possible obscured quasars with 90% $L_{2-10keV}$ uncertainty range across 10^{44} erg s $^{-1}$ (12 with $N_H > 10^{22}$ cm $^{-2}$ at $> 90\%$ confidence level, XID 51,54,152,156,209,227,243,253,259,263,543,601,609), the upper limit of the fraction could be 84%. We can clearly see that due to the large uncertainties in the measurement of both N_H and $L_{2-10keV}$, the fraction of obscured quasars in CDF-S ranges from 54% to 84%. If we simply adopt the best-fit N_H and $L_{2-10keV}$, the fraction is 71% (20 out 28). Apply the same selection criteria to table 1 in T06 (with best-fit $N_H > 10^{22}$ and $L_{2-10keV} > 10^{44}$ erg s $^{-1}$), we obtain a slightly higher fraction of 85% (39 out 46, but consistent within 1σ uncertainty). Considering that most of our 4 – 7 keV band selected sources are among the brightest in the CDF-S sample (see Fig. 2), and since the absorbed fraction is increasing at lower fluxes, two values well agree with each other.

Among the 13 secure obscured quasars and 18 extra possible obscured quasars, we find optical classification for 19 of them from Szokoly et al. (2004). Only three (XID 24,62,68) are classified as broad line AGN, and all of them show associated absorption systems in their optical spectra (XID 62 is identified as BAL QSO), suggesting an outflow origin for their X-ray obscuration. This indicates that most of our X-ray obscured quasars are likely type II QSO with broad line region also obscured.

In CDF-N, we obtained 21 quasars with best-fit $L_{2-10keV} > 10^{44}$ erg s $^{-1}$, 6 of which have best-fit $N_H > 10^{22}$ cm $^{-2}$, corresponding to a much smaller fraction of 29%. However we note that the total number of quasars in CDF-N (21) is much less than that in CDF-S (28) although CDF-N is twice as deep and is expected to detect more quasars. This is a consequence of the fact that a significant fraction of the quasars have no redshift available. In

Fig. 6 we plot the redshift distribution of the 4 – 7 keV band sources in CDF-S and CDF-N. Assuming that the CDF-N sample has similar redshift distribution to that of CDF-S sample, we can see in the figure that most of the sources without redshifts in CDF-N should locate at redshift between 1 and 4. Assuming all sources without redshifts in CDF-N are located at $z = 2$ (or 3), we perform spectral fitting to estimate their N_H and $L_{2-10keV}$. After such a coarse correction to redshift incompleteness, we find the fraction of obscured quasars could increase to 50% (or 63%) and the total number of quasars could increase to 31 (or 41).

5. Conclusions

We present 4 – 7 keV band selected sources in CDF-S. We find that 54% – 84% of the 4 – 7 keV band quasars in CDF-S are obscured with $N_H > 10^{22} \text{ cm}^{-2}$. This result is well consistent with that of Dwelly & Page (2006) who find that $\sim 75\%$ XMM-Newton sources in CDF-S are obscured at all luminosities. We also note that a most recent work by Georgantopoulo, Georgakakis & Akylas (2006) obtained a similar fraction of X-ray obscured quasars in CDF-S (74%, 17 out of 23) by fitting X-ray spectra of 186 2 – 10 keV band detected sources covered by all 11 *Chandra* pointings. We indicate that using different versions of *Chandra* calibrations yield consistent fitting results, suggesting that calibration uncertainty would not significantly affect our main results presented in this paper. The uncertainties in the measurement of both L_X and N_H are also carefully taken into account. We note that AGN’s X-ray spectra are often more complicated than an absorbed powerlaw model (T06), especially in the soft band (such as warm absorber and soft excess), however we note that most of the quasars are located at high redshift ($z > 1$) for which extra soft features would have been shifted out of *Chandra* bandpass. In CDF-N, the fraction is much lower (29%), however, we found this is probably due to the redshift incompleteness in the CDF-N sample. After correcting the redshift completeness, we found that 50%-63% of the quasars in CDF-N are obscured, consistent with that in CDF-S (54% - 84%). Our results robustly confirm the existence of a large population of obscured quasars.

The work of JW was supported by Chinese NSF through NSFC10473009, NSFC10533050 and the CAS "Bai Ren" project at University of Science and Technology of China. PT acknowledges financial contribution from contract ASI-INAF I/023/05/0.

REFERENCES

- Alexander, D. M., et al. 2003, *AJ*, 126, 539
- Antonucci, R. 1993, *ARA&A*, 31, 473
- Barger, A. J., et al. 2005, *ApJ*, 129, 578
- Brandt, W. N., et al. 2001, *AJ*, 122, 2810
- Caccianiga, A., et a. 2004, *A&A*, 416, 901
- Cash, W. 1979, *ApJ*, 228, 939
- Comastri, A., Fiore, F., Vignali, C., Matt, G., Perola, G. C. & La Franca, F. 2001, *MNRAS*, 327, 781
- Dickey, L. M., & Lockman, F. J. 1990, *ARA&A*, 28, 215
- Dwelly, T. et al. 2005, *MNRAS*, 360, 1426
- Dwelly, T. & Page, M. J. 2006, *MNRAS* in press, astro-ph0608479
- Eckart, M. E. et al. 2006, *ApJ* in press, astro-ph0603556
- Fiore, F. et al. 1999, *MNRAS*, 306, L55
- Fiore, F. et al. 2003, *A&A*, 409, 79
- Freeman, P. E., Kashyap, V., Rosner, R., Lamb, D. Q. 2002, *ApJS*, 138, 185
- Geheres, N, 1986, *ApJ*, 303, 336
- Georgantopoulo, I., Georgakakis, A. & Akylas, A. 2006, *A&A* accepted, astro-ph/0610828
- Giacconi, R., et al. 2001, *ApJ*, 511, 624
- Giacconi, R., et al. 2002, *ApJS*, 139, 369
- Kormendy, J., & Gebhardt, K. 2001, in *AIP Conf. Proc.* 586, 20th Texas Symposium on Relativistic Astrophysics, ed. H. Martel & J. C. Wheeler (Melville: AIP), 363
- Kormendy, J., & Richstone, D. 1995, *ARA&A*, 33, 581
- La Franca, F. et al. 2005, *ApJ*, 635, 864
- Mainieri, V. et al. 2002, *A&A*, 393, 425
- Martínez-Sansigre, A. et al. 2005, *Nature*, 436, 666
- Nandra, K., Georgantopoulos, I., Ptak, A., & Turner, T. J. 2003, *ApJ*, 582, 615
- Norman, C. A. et al. 2002, *ApJ*, 571, 218
- Perola, G. C. et al. 2004, *A&A*, 421, 491

- Piconcelli, E., Cappi, M., Bassani, L., Fiore, F., Di Cocco, G., Stephen, J. B. 2002, *A&A* 394, 835
- Piconcelli, E., Cappi, M., Bassani, L., Di Cocco, G., Dadina, M. 2003, *A&A*, 412, 689
- Rosati, P. et al. 2002, *ApJ*, 566, 667
- Spergel, D. N. et al. 2003, *ApJS*, 148, 175
- Steffen, A. T., Barger, A. J., Cowie, L. L., Mushotzky, R. F., Yang, Y. 2003, *ApJ*, 596, L23
- Stern, D. et al. 2002, *ApJ*, 568, 71
- Szokoly, G. P., et al. 2004, *ApJS*, 155, 271
- Tozzi, P, et al. 2001, *ApJ*, 562, 42
- Tozzi, P, et al. 2006, *A&A*, 451, 457, T06
- Ueda, Y., Akiyama, M., Ohta, K., Miyaji, T. 2003, *ApJ*, 598, 886
- Yu, Q. & Tremaine, S. 2002, *MNRAS*, 336, 965
- Zheng, W. et al. 2004, *ApJS*, 155, 73

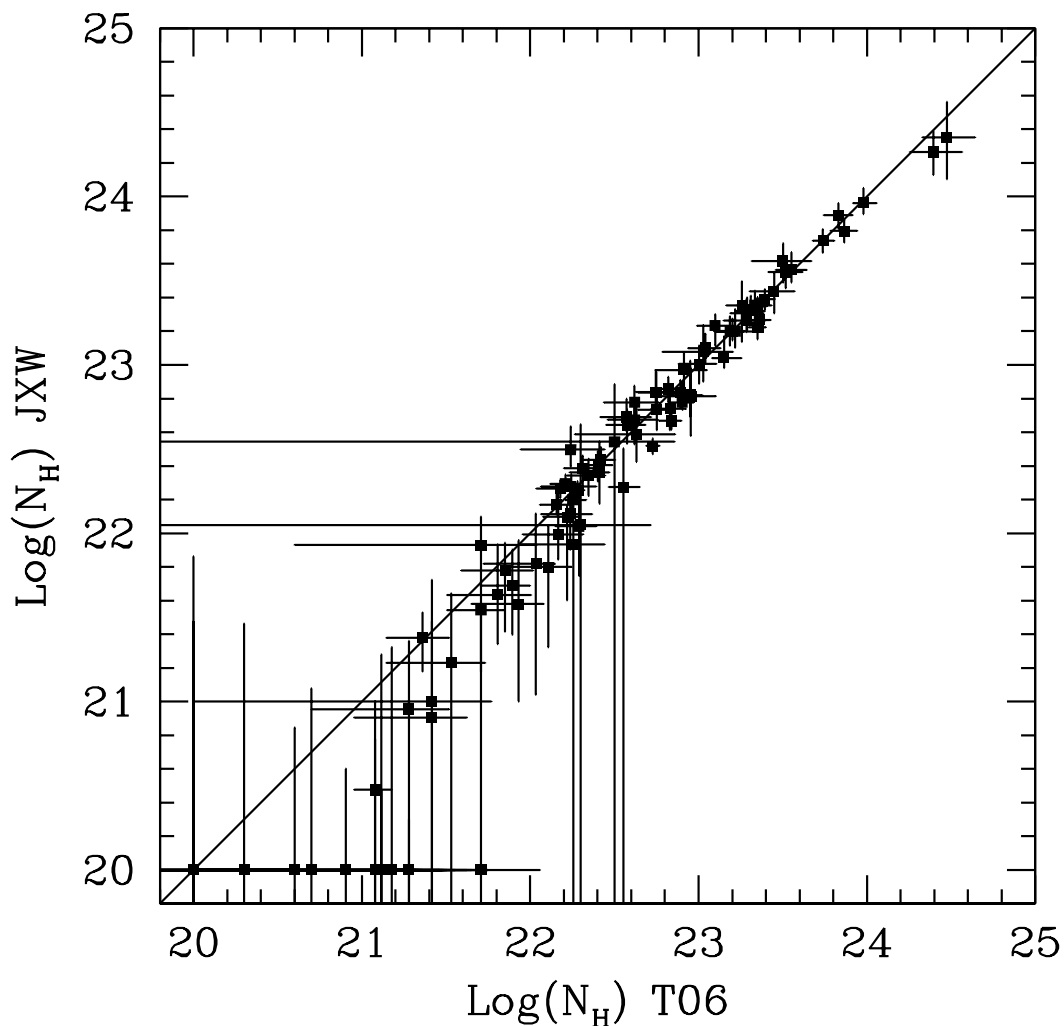


Fig. 1.— The best-fit absorption column densities (with 1σ errorbars) from X-ray spectra with different version of Chandra calibrations. The X axis plots N_H from T06 (with CALDB2.26) and the Y axis plots the independently derived N_H from re-calibrated spectra (with CALDB3.1.0). For display purpose, we plot best-fit $N_H=0$ at $N_H = 10^{22} \text{ cm}^{-2}$. For faint sources in T06 for which Γ was fixed at 1.8, we adopted the same fixed Γ in this figure.

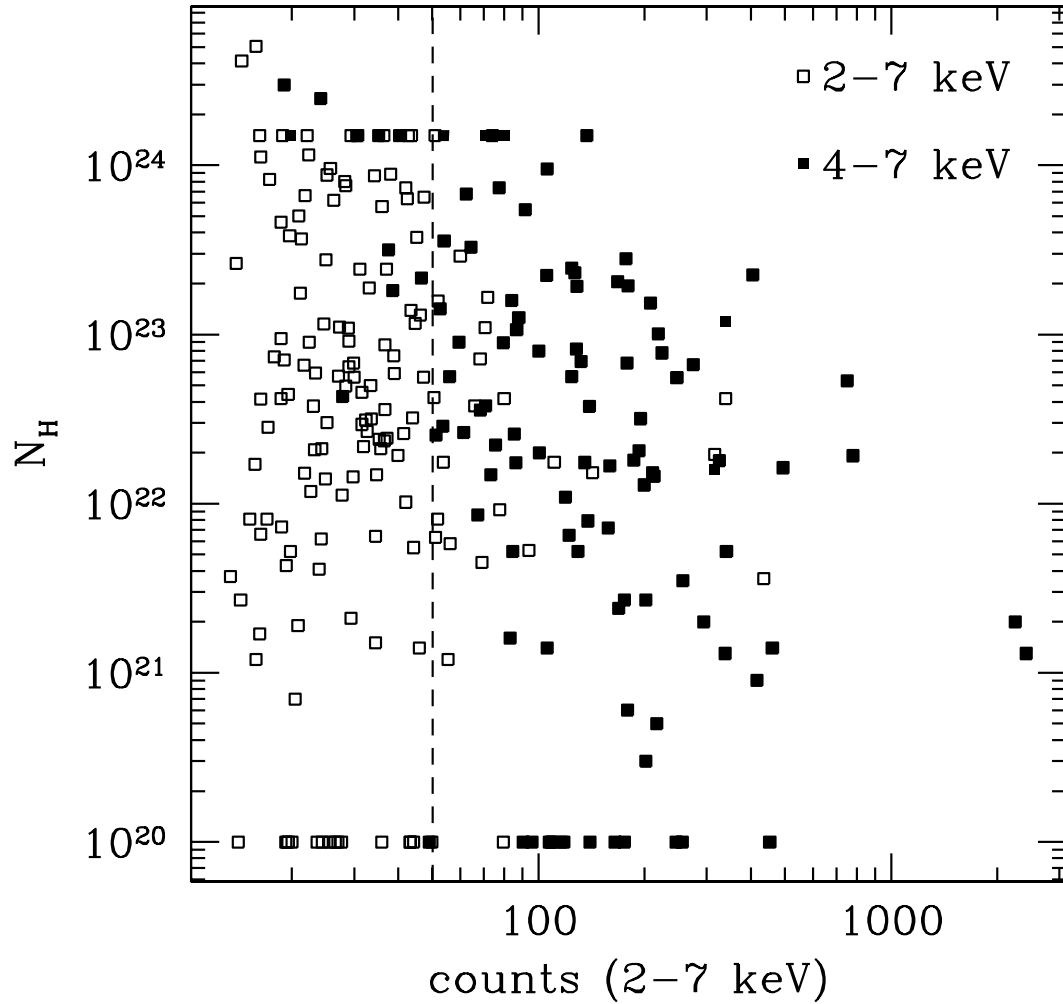


Fig. 2.— The X-ray absorption column density N_H of the 2 – 7 keV selected AGNs in CDF-S versus the X-ray counts in 2 – 7 keV detected by *Chandra* (open squares). The 4 – 7 keV detected sources are overplotted as solid squares. To the right of the dashed vertical line, the total number of sources is 107, the same as that of the 4 – 7 keV selected sources.

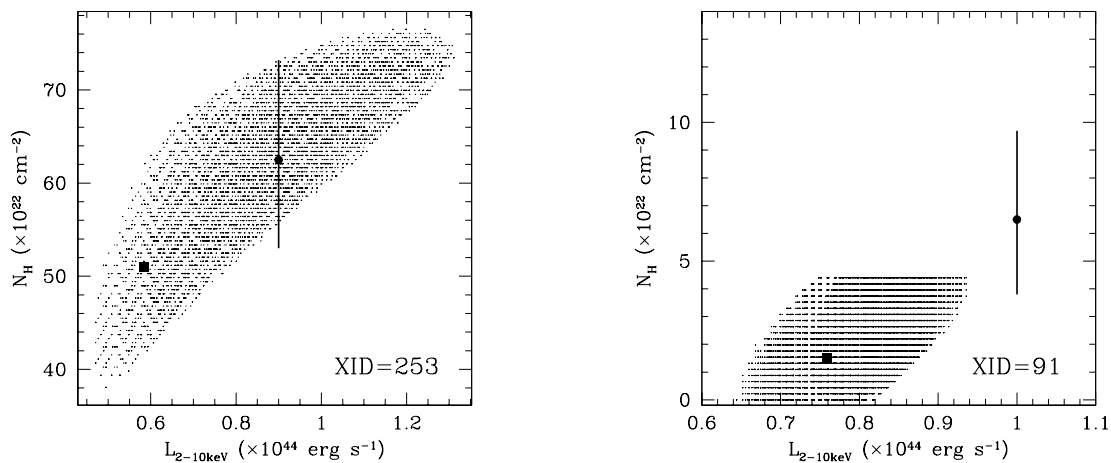


Fig. 3.— The 90% confidence range ($\Delta C=2.706$) of N_H and L_X for two possible obscured quasars. The confidence range was calculated by setting the photon index Γ varying from 1.4 to 2.4 with best-fit N_H and L_X marked as black squares. The best-fit values with Γ fixed at 1.8 are also plotted as black dots with 90% errorbars for N_H (solid line).

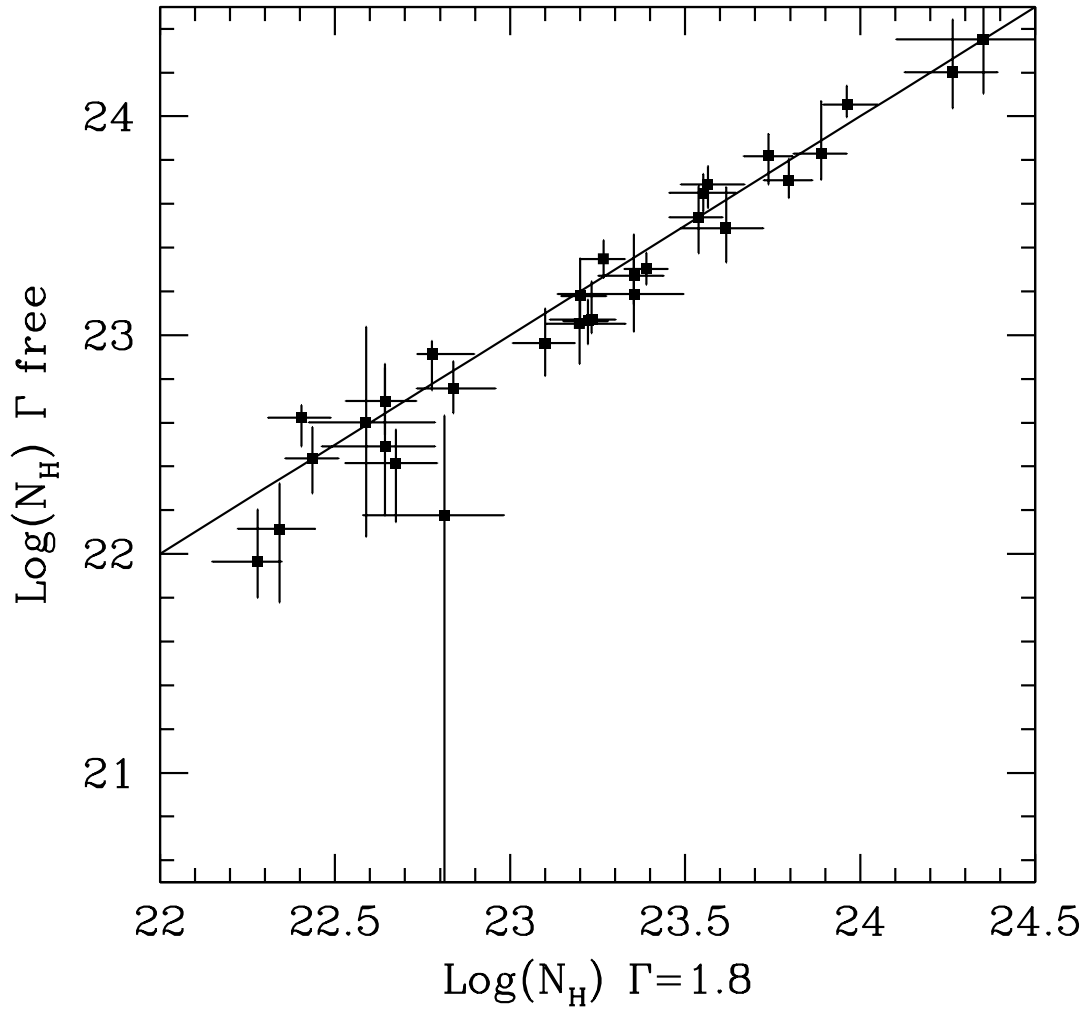


Fig. 4.— The best-fit absorption column density (with 1σ errorbars) with Γ free versus that with Γ fixed at 1.8 for faint sources in 4 – 7 keV band sample. The solid line plots $X = Y$.

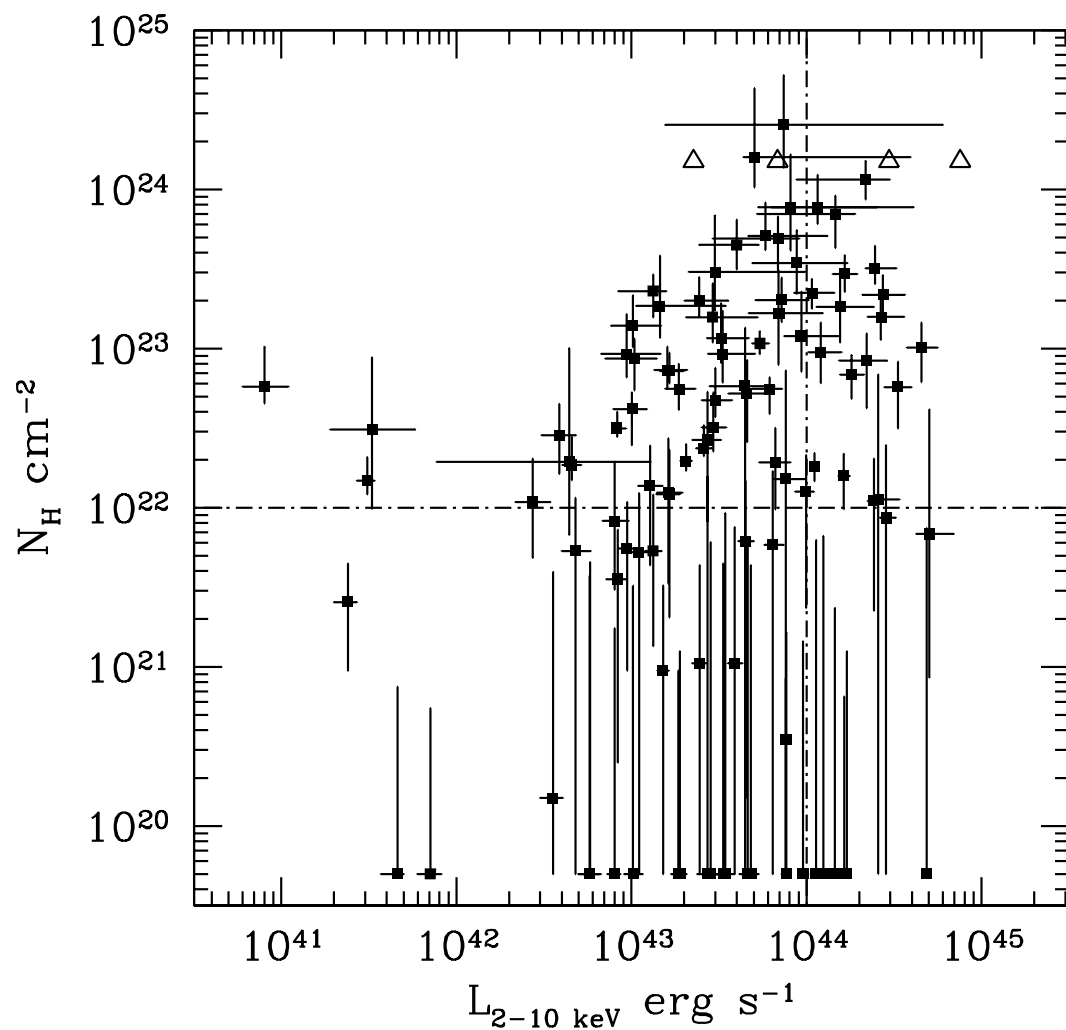


Fig. 5.— Our best-fit absorption column density versus absorption corrected $L_{2-10\text{keV}}$ with 90% errorbars for 107 4 – 7 keV band selected sources in CDF-S. All data are from table 1. Triangles are sources fitted with reflection model (*pexrav*, see table 1 for details). For display purpose, we assign $0.5 \times 10^{20} \text{ cm}^{-2}$ to sources with best-fit N_H at zero. Our selection criteria for obscured quasars are plotted as dash-dotted lines.

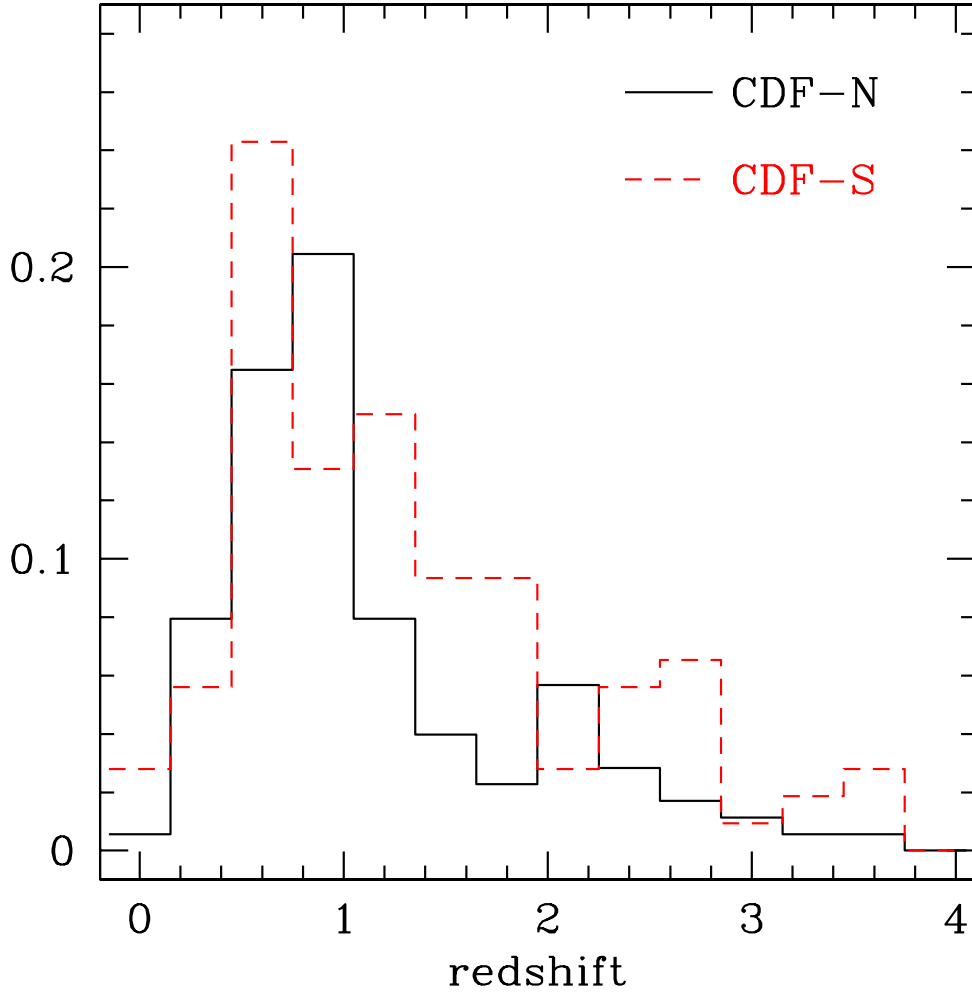


Fig. 6.— The fractional redshift distribution of our 4 – 7 keV band selected sources in CDF-S (dashed line) and CDF-N (solid line). Note the redshift completeness for CDF-S sample is 100% and 72% for CDF-N sample.

Table 1. X-ray spectral fits to 4 – 7 keV selected sources in CDF-S

XID	z	Q	$N_H/10^{22} \text{ cm}^{-2}$	Γ	$L_{2-10 \text{ keV}} \text{ erg s}^{-1}$
22	1.92	3.0	$0.00^{+0.66}_{-0.00}$	$1.81^{+0.16}_{-0.11}$	$1.25^{+0.08}_{-0.08} \times 10^{44}$
27	3.06	3.0	$31.85^{+12.20}_{-6.33}$	$1.40^{+0.17}_{-0.00}$	$2.45^{+0.81}_{-0.28} \times 10^{44}$
39	1.22	3.0	$0.00^{+0.14}_{-0.00}$	$1.78^{+0.07}_{-0.08}$	$9.54^{+0.41}_{-0.47} \times 10^{43}$
202	3.70	3.0	150	$2.12^{+0.25}_{-0.22}$	7.53×10^{44}
151	0.60	3.0	$22.94^{+6.26}_{-7.21}$	$2.40^{+0.00}_{-0.77}$	$1.33^{+0.25}_{-0.49} \times 10^{43}$
153	1.54	3.0	150	$1.55^{+0.26}_{-0.15}$	2.69×10^{44}
63	0.54	3.0	$0.03^{+0.05}_{-0.03}$	$1.86^{+0.06}_{-0.04}$	$7.60^{+0.15}_{-0.23} \times 10^{43}$
256	1.53	0.5	$49.24^{+18.16}_{-18.31}$	$2.40^{+0.00}_{-0.93}$	$6.88^{+2.23}_{-3.98} \times 10^{43}$
26	1.65	0.5	$5.20^{+3.24}_{-2.61}$	$1.95^{+0.45}_{-0.42}$	$4.57^{+1.54}_{-0.99} \times 10^{43}$
79	1.82	0.5	$0.00^{+1.58}_{-0.00}$	$1.71^{+0.42}_{-0.27}$	$2.71^{+0.58}_{-0.35} \times 10^{43}$
31	1.60	3.0	$1.58^{+0.61}_{-0.61}$	$2.10^{+0.14}_{-0.16}$	$1.63^{+0.13}_{-0.11} \times 10^{44}$
36	1.03	0.5	$1.37^{+1.08}_{-0.94}$	$1.99^{+0.41}_{-0.37}$	$1.27^{+0.23}_{-0.19} \times 10^{43}$
38	0.74	3.0	$0.00^{+0.09}_{-0.00}$	$1.94^{+0.10}_{-0.10}$	$1.84^{+0.14}_{-0.13} \times 10^{43}$
42	0.73	3.0	$0.00^{+0.06}_{-0.00}$	$1.93^{+0.05}_{-0.04}$	$1.64^{+0.05}_{-0.03} \times 10^{44}$
145	1.50	0.5	$11.57^{+7.69}_{-3.45}$	$1.40^{+0.50}_{-0.00}$	$3.25^{+1.43}_{-0.56} \times 10^{43}$
51	1.10	3.0	$22.34^{+5.02}_{-4.58}$	$1.77^{+0.38}_{-0.37}$	$1.07^{+0.37}_{-0.23} \times 10^{44}$
53	0.68	3.0	$0.00^{+0.37}_{-0.00}$	$1.63^{+0.29}_{-0.17}$	$5.75^{+0.80}_{-0.70} \times 10^{42}$
55	0.12	3.0	$1.47^{+0.60}_{-0.26}$	$1.43^{+0.39}_{-0.03}$	$3.10^{+0.30}_{-0.40} \times 10^{41}$
257	0.55	1.5	150	$1.89^{+0.49}_{-0.49}$	2.26×10^{43}
62	2.81	3.0	$21.81^{+7.05}_{-6.50}$	$1.81^{+0.30}_{-0.29}$	$2.73^{+0.93}_{-0.66} \times 10^{44}$
64	0.13	0.4	$0.25^{+0.19}_{-0.16}$	$1.74^{+0.27}_{-0.23}$	$2.40^{+0.30}_{-0.40} \times 10^{41}$
259	1.76	0.5	$69.81^{+21.58}_{-26.97}$	$2.33^{+0.07}_{-0.88}$	$1.46^{+0.44}_{-0.94} \times 10^{44}$
18	0.98	3.0	$1.82^{+0.38}_{-0.36}$	$1.77^{+0.13}_{-0.12}$	$1.11^{+0.06}_{-0.06} \times 10^{44}$
147	0.99	0.5	$19.97^{+8.17}_{-4.13}$	$1.40^{+0.58}_{-0.00}$	$2.44^{+1.12}_{-0.43} \times 10^{43}$
20	1.02	3.0	$5.56^{+2.43}_{-1.44}$	$1.60^{+0.44}_{-0.20}$	$1.87^{+0.45}_{-0.30} \times 10^{43}$
28	1.22	3.0	$1.24^{+1.48}_{-0.91}$	$1.46^{+0.41}_{-0.06}$	$1.63^{+0.33}_{-0.23} \times 10^{43}$
33	0.67	3.0	$0.09^{+0.23}_{-0.09}$	$1.59^{+0.16}_{-0.13}$	$1.51^{+0.12}_{-0.11} \times 10^{43}$
148	1.74	0.5	$9.23^{+7.92}_{-3.11}$	$1.47^{+0.58}_{-0.07}$	$3.30^{+1.75}_{-0.57} \times 10^{43}$
515	2.28	0.5	$30.20^{+39.02}_{-12.96}$	$1.40^{+0.95}_{-0.00}$	$3.00^{+6.87}_{-0.87} \times 10^{43}$
78	0.96	3.0	$0.00^{+0.32}_{-0.00}$	$2.05^{+0.24}_{-0.19}$	$1.02^{+0.14}_{-0.11} \times 10^{43}$
81	2.59	0.5	$5.81^{+7.69}_{-5.81}$	$2.03^{+0.37}_{-0.62}$	$4.44^{+2.09}_{-1.64} \times 10^{43}$
253	1.89	1.9	$51.03^{+31.53}_{-9.41}$	$1.40^{+0.76}_{-0.00}$	$5.83^{+7.29}_{-1.20} \times 10^{43}$
254	0.10	0.7	$5.73^{+4.52}_{-1.22}$	$1.40^{+0.89}_{-0.00}$	$8.00^{+3.00}_{-2.00} \times 10^{40}$
50	0.67	1.9	$1.08^{+0.54}_{-0.60}$	$1.40^{+0.18}_{-0.00}$	$2.73^{+0.70}_{-0.55} \times 10^{42}$
52	0.57	3.0	$0.00^{+0.17}_{-0.00}$	$1.96^{+0.17}_{-0.10}$	$7.99^{+0.66}_{-0.73} \times 10^{42}$
56	0.60	3.0	$1.96^{+0.55}_{-0.26}$	$1.40^{+0.19}_{-0.00}$	$2.05^{+0.17}_{-0.14} \times 10^{43}$
60	1.61	3.0	$0.00^{+0.23}_{-0.00}$	$1.88^{+0.09}_{-0.09}$	$1.44^{+0.08}_{-0.95} \times 10^{44}$
227	2.18	0.5	$77.15^{+46.04}_{-16.24}$	$1.79^{+0.61}_{-0.39}$	$1.15^{+1.38}_{-0.53} \times 10^{44}$
66	0.57	3.0	$7.22^{+2.21}_{-1.18}$	$1.59^{+0.44}_{-0.19}$	$1.65^{+0.34}_{-0.19} \times 10^{43}$
67	1.62	3.0	$0.00^{+0.62}_{-0.00}$	$1.65^{+0.14}_{-0.11}$	$1.13^{+0.07}_{-0.07} \times 10^{44}$
70	1.07	0.4	$10.77^{+2.11}_{-1.61}$	$1.40^{+0.09}_{-0.00}$	$5.41^{+0.69}_{-0.53} \times 10^{43}$
4	1.26	1.6	$0.00^{+0.57}_{-0.00}$	$1.74^{+0.22}_{-0.11}$	$4.59^{+0.28}_{-0.46} \times 10^{43}$
6	2.46	0.2	$0.86^{+1.60}_{-0.86}$	$1.89^{+0.21}_{-0.17}$	$2.84^{+0.38}_{-0.22} \times 10^{44}$
11	2.58	3.0	$0.00^{+0.74}_{-0.00}$	$1.84^{+0.12}_{-0.08}$	$4.84^{+0.30}_{-0.24} \times 10^{44}$
152	1.28	0.6	$20.20^{+7.62}_{-5.56}$	$1.81^{+0.59}_{-0.41}$	$7.18^{+3.10}_{-2.08} \times 10^{43}$
159	3.30	0.5	$10.14^{+4.47}_{-3.98}$	$1.68^{+0.20}_{-0.20}$	$4.52^{+1.10}_{-0.79} \times 10^{44}$

Table 1—Continued

XID	z	Q	$N_H/10^{22}\text{cm}^{-2}$	Γ	$L_{2-10\text{keV}}\text{ erg s}^{-1}$
91	3.19	1.0	$1.51^{+5.75}_{-1.51}$	$1.40^{+0.31}_{-0.00}$	$7.59^{+2.28}_{-1.10} \times 10^{43}$
24	3.61	3.0	$1.12^{+5.77}_{-1.12}$	$1.56^{+0.28}_{-0.16}$	$2.57^{+0.83}_{-0.29} \times 10^{44}$
29	0.30	0.9	$3.14^{+0.87}_{-0.35}$	$1.55^{+0.36}_{-0.15}$	$8.27^{+1.05}_{-0.46} \times 10^{42}$
265	1.22	1.5	$15.71^{+9.94}_{-4.76}$	$1.78^{+0.62}_{-0.38}$	$2.91^{+2.35}_{-0.85} \times 10^{43}$
264	1.32	1.9	$18.49^{+19.80}_{-6.83}$	$1.45^{+0.95}_{-0.05}$	$1.45^{+1.99}_{-0.39} \times 10^{43}$
44	1.03	3.0	$0.00^{+0.16}_{-0.00}$	$2.26^{+0.11}_{-0.06}$	$7.67^{+0.28}_{-0.46} \times 10^{43}$
45	2.29	1.5	$9.44^{+5.16}_{-3.39}$	$1.57^{+0.36}_{-0.17}$	$1.20^{+0.38}_{-0.18} \times 10^{44}$
531	1.54	3.0	150	1.80^f	6.83×10^{43}
156	1.19	3.0	$115.65^{+35.11}_{-29.02}$	$2.40^{+0.00}_{-0.77}$	$2.18^{+0.82}_{-1.30} \times 10^{44}$
59	0.97	0.5	$2.35^{+0.94}_{-0.25}$	$1.78^{+0.27}_{-0.26}$	$2.59^{+0.31}_{-0.25} \times 10^{43}$
61	2.02	0.5	$1.10^{+0.92}_{-0.88}$	$1.84^{+0.16}_{-0.15}$	$2.42^{+0.22}_{-0.19} \times 10^{44}$
68	2.73	3.0	$5.72^{+2.57}_{-2.58}$	$1.96^{+0.20}_{-0.21}$	$3.31^{+0.67}_{-0.53} \times 10^{44}$
72	1.99	0.5	$6.82^{+2.26}_{-2.00}$	$1.84^{+0.25}_{-0.24}$	$1.80^{+0.33}_{-0.25} \times 10^{44}$
10	0.42	3.0	$1.85^{+0.93}_{-0.36}$	$1.40^{+0.31}_{-0.00}$	$4.55^{+0.60}_{-0.51} \times 10^{42}$
15	1.23	1.5	$0.10^{+0.65}_{-0.10}$	$1.72^{+0.27}_{-0.13}$	$3.89^{+0.40}_{-0.33} \times 10^{43}$
19	0.74	3.0	$0.10^{+0.33}_{-0.10}$	$1.82^{+0.23}_{-0.14}$	$2.45^{+0.23}_{-0.23} \times 10^{43}$
146	2.67	0.5	$1.92^{+1.25}_{-0.95}$	$1.40^{+0.27}_{-0.00}$	$6.62^{+1.49}_{-1.27} \times 10^{43}$
201	0.68	3.0	$2.84^{+1.64}_{-1.21}$	$1.85^{+0.55}_{-0.45}$	$3.86^{+0.97}_{-0.80} \times 10^{42}$
41	0.67	3.0	$7.30^{+2.98}_{-1.69}$	$1.66^{+0.56}_{-0.26}$	$1.61^{+0.47}_{-0.26} \times 10^{43}$
150	1.09	3.0	$44.73^{+19.89}_{-13.23}$	$2.40^{+0.00}_{-0.61}$	$3.99^{+1.35}_{-1.55} \times 10^{43}$
46	1.62	3.0	$0.58^{+1.11}_{-0.58}$	$2.04^{+0.34}_{-0.21}$	$6.40^{+1.02}_{-0.67} \times 10^{43}$
47	0.73	3.0	$8.63^{+2.90}_{-3.16}$	$2.30^{+0.10}_{-0.75}$	$1.04^{+0.36}_{-0.33} \times 10^{43}$
49	0.53	3.0	$0.01^{+0.38}_{-0.01}$	$1.70^{+0.34}_{-0.18}$	$3.55^{+0.50}_{-0.55} \times 10^{42}$
263	3.66	3.0	$77.22^{+88.80}_{-35.88}$	$1.41^{+0.99}_{-0.01}$	$8.07^{+32.89}_{-2.77} \times 10^{43}$
206	1.32	3.0	$0.00^{+0.12}_{-0.00}$	$2.06^{+0.08}_{-0.08}$	$1.69^{+0.07}_{-0.07} \times 10^{44}$
57	2.56	3.0	$18.31^{+10.88}_{-7.38}$	$1.65^{+0.42}_{-0.25}$	$1.55^{+0.87}_{-0.42} \times 10^{44}$
58	0.92	0.5	$4.16^{+1.12}_{-1.69}$	$2.40^{+0.00}_{-0.53}$	$1.01^{+0.22}_{-0.22} \times 10^{43}$
538	0.31	3.0	$3.09^{+5.69}_{-2.11}$	$1.40^{+1.00}_{-0.00}$	$3.30^{+2.50}_{-1.40} \times 10^{41}$
114	1.72	0.5	$2.66^{+2.69}_{-1.85}$	$1.40^{+0.23}_{-0.00}$	$2.71^{+0.53}_{-0.49} \times 10^{43}$
99	0.79	0.5	$0.53^{+0.67}_{-0.40}$	$1.50^{+0.29}_{-0.10}$	$1.33^{+0.16}_{-0.14} \times 10^{43}$
73	0.73	3.0	$0.55^{+0.53}_{-0.46}$	$1.70^{+0.28}_{-0.28}$	$9.41^{+1.12}_{-1.00} \times 10^{42}$
76	2.39	1.2	$15.78^{+6.06}_{-4.43}$	$1.63^{+0.35}_{-0.22}$	$2.66^{+0.95}_{-0.43} \times 10^{44}$
208	0.72	0.6	$0.53^{+0.62}_{-0.53}$	$2.00^{+0.40}_{-0.42}$	$4.79^{+1.04}_{-0.80} \times 10^{42}$
501	0.81	0.6	$0.00^{+0.60}_{-0.00}$	$1.73^{+0.24}_{-0.14}$	$2.82^{+0.27}_{-0.23} \times 10^{43}$
12	0.25	3.0	$0.00^{+0.05}_{-0.00}$	$1.95^{+0.18}_{-0.15}$	$7.10^{+1.10}_{-1.10} \times 10^{41}$
25	2.26	0.5	$29.47^{+9.03}_{-6.74}$	$1.40^{+0.09}_{-0.00}$	$1.65^{+0.30}_{-0.24} \times 10^{44}$
609	1.86	0.5	$159.25^{+273.38}_{-56.16}$	$1.40^{+1.00}_{-0.00}$	$5.03^{+34.16}_{-0.66} \times 10^{43}$
190	0.73	3.0	$13.89^{+7.62}_{-3.65}$	$1.40^{+0.69}_{-0.00}$	$1.02^{+0.46}_{-0.25} \times 10^{43}$
34	0.84	3.0	$0.52^{+0.71}_{-0.52}$	$1.58^{+0.32}_{-0.18}$	$1.10^{+0.14}_{-0.14} \times 10^{43}$
203	1.17	0.7	$0.61^{+0.85}_{-0.60}$	$1.50^{+0.28}_{-0.10}$	$4.47^{+0.52}_{-0.41} \times 10^{43}$
601	0.73	3.0	$255.19^{+265.46}_{-118.40}$	$2.26^{+0.14}_{-0.86}$	$7.39^{+52.79}_{-5.83} \times 10^{43}$
83	1.76	0.5	$0.00^{+0.92}_{-0.00}$	$1.40^{+0.35}_{-0.00}$	$3.43^{+0.42}_{-0.39} \times 10^{43}$
543	1.81	0.5	$34.53^{+21.09}_{-12.40}$	$1.80^{+0.60}_{-0.40}$	$8.76^{+8.37}_{-3.85} \times 10^{43}$
13	0.73	3.0	$0.00^{+0.12}_{-0.00}$	$1.83^{+0.18}_{-0.13}$	$1.89^{+0.18}_{-0.21} \times 10^{43}$
200	0.85	0.4	$0.82^{+1.12}_{-0.52}$	$1.40^{+0.30}_{-0.00}$	$8.02^{+1.60}_{-1.18} \times 10^{42}$
30	0.84	3.0	$0.00^{+0.43}_{-0.00}$	$1.87^{+0.28}_{-0.15}$	$4.80^{+0.51}_{-0.55} \times 10^{43}$

Table 1—Continued

XID	z	Q	$N_H/10^{22} \text{cm}^{-2}$	Γ	$L_{2-10\text{keV}} \text{ erg s}^{-1}$
35	1.51	3.0	$8.36^{+4.09}_{-4.13}$	$2.05^{+0.35}_{-0.55}$	$2.21^{+0.66}_{-0.68} \times 10^{44}$
48	1.26	0.5	$3.20^{+2.08}_{-0.95}$	$1.40^{+0.34}_{-0.00}$	$2.92^{+0.57}_{-0.40} \times 10^{43}$
54	2.56	3.0	$11.97^{+10.69}_{-4.83}$	$1.53^{+0.58}_{-0.13}$	$9.34^{+5.84}_{-1.87} \times 10^{43}$
97	0.18	2.0	$0.00^{+0.07}_{-0.00}$	$1.41^{+0.23}_{-0.01}$	$4.60^{+0.40}_{-0.90} \times 10^{41}$
207	0.40	0.4	$5.57^{+1.01}_{-1.69}$	$2.40^{+0.00}_{-0.68}$	$6.14^{+1.13}_{-1.25} \times 10^{43}$
65	1.10	0.5	$1.21^{+1.09}_{-1.01}$	$1.96^{+0.44}_{-0.41}$	$1.65^{+0.25}_{-0.26} \times 10^{43}$
71	1.04	3.0	$0.00^{+0.44}_{-0.00}$	$1.72^{+0.19}_{-0.12}$	$3.34^{+0.28}_{-0.29} \times 10^{43}$
75	0.74	3.0	$4.71^{+2.82}_{-1.00}$	$1.41^{+0.58}_{-0.01}$	$3.01^{+0.75}_{-0.48} \times 10^{43}$
7	1.84	0.6	$0.68^{+3.48}_{-0.60}$	$1.70^{+0.35}_{-0.12}$	$5.04^{+1.90}_{-0.82} \times 10^{44}$
23	0.73	0.5	$0.00^{+0.45}_{-0.00}$	$1.84^{+0.33}_{-0.19}$	$5.79^{+0.90}_{-0.84} \times 10^{42}$
243	2.50	0.3	$16.66^{+14.60}_{-8.74}$	$1.40^{+0.64}_{-0.00}$	$6.91^{+5.50}_{-2.22} \times 10^{43}$
267	0.72	1.2	$9.24^{+7.20}_{-2.67}$	$1.40^{+0.81}_{-0.00}$	$9.36^{+5.30}_{-2.64} \times 10^{42}$
213	0.60	0.5	$1.94^{+8.09}_{-1.27}$	$1.42^{+0.98}_{-0.02}$	$4.41^{+8.45}_{-3.64} \times 10^{42}$
209	1.32	0.5	$1.26^{+0.88}_{-1.03}$	$1.55^{+0.33}_{-0.15}$	$9.91^{+1.13}_{-1.29} \times 10^{43}$
503	0.54	0.4	$0.35^{+0.37}_{-0.33}$	$1.87^{+0.31}_{-0.29}$	$8.32^{+1.04}_{-1.14} \times 10^{42}$

Note. — The table lists in turn XID, redshift and its quality (see Zheng et al. 2004), best fit N_H , powerlaw photon index Γ and 2 – 10 keV rest frame absorption corrected luminosity. Following T06, 0.6 – 7 keV band spectra are adopted (binned to at least 1 photon per bin) for spectral fit, and C-statistic (Cash 1979) for minimization. All the quoted errors are 90% confidence range for one parameter of interest. The primary model is an absorbed powerlaw with Galactic absorption included. The uncertainties of luminosities are estimated by varying Γ , N_H and powerlaw normalization to include parameter sets with $\Delta C < 2.706$. The varying range of Γ is set to 1.4 to 2.4 (see text for details). Sources with N_H fixed at 1.5×10^{24} are better fitted (with $\Delta C < -4$) by the reflection model (*pxravl*) and its intrinsic luminosities are estimated assuming the reflected luminosity in 2 – 10 keV band is about 6% of the intrinsic one (see T06 for details for spectral models and fitting procedures).